Electronic Supplementary Information

Ultrafast ultrasound-assisted synthesis of microporous organic networks for the efficient removal of antibiotics

Hua-Xing Liu,[a] Yuan-Yuan Cui,[b] Abdukader Abdukayum,*[a] Cheng-Xiong Yang*[b]

[a] Xinjiang Key Laboratory of Novel Functional Materials Chemistry, Laboratory of Xinjiang Native Medicinal and Edible Plant Resources Chemistry, College of Chemistry and Environmental Sciences, Kashi University, Kashi 844000, China.

[b] School of Pharmaceutical Sciences & Institute of Materia Medica, Medical Science and Technology Innovation Center, Shandong First Medical University & Shandong Academy of Medical Sciences, Jinan, Shandong 250117, China.

*Corresponding author.

E-mail: cxyang@nankai.edu.cn

Chemicals, reagents and instruments

All reagents used were at least of analytical grade. The ultrapure water was obtained from Wahaha Food Co., Ltd. (Hangzhou, China). Tetrakis(4-ethynylphenyl)methane was purchased from Chengdu Tongchuangyuan Pharmaceutical Technology Co. Ltd. (Chengdu, China). 1,4-Dibromobenzene and 2,5-dibromhydroquinone were obtainable from EnerTech Chemical. (Shanghai China). Copper(I) iodide was supplied by Sigma-Aldrich Trading Co., Ltd. (Shanghai, China). Bis(triphenylphos-phine)palladium dichloride was purchased from Sane Chemical Technology Co., Ltd (Shanghai, China). The *N,N*-dimethyl-formamide (DMF), triethylamine, methanol, acetonitrile, toluene and ethanol were obtained from Concord Co., Ltd. (Tianjin, China). The 2,5-dibromop-phenylenediamine was provided by Warwick Reek Chemistry. Tetracycline hydrochloride (TCH) was acquired from Aladdin Chemistry Co., Ltd. (Shanghai, China). Oxalic acid was purchased from Yuanye Bio-Technology Co., Ltd (Shanghai, China). Formic acid (FA), ciprofloxacin (CIP), enrofloxacin (ENR), ofloxacin (OFL), enoxacin (ENO), cefotaxime sodium, cefixime, cefuroxime sodium, cefazolin sodium salt, dichlorprop, 2,4-dichlorophenoxyacetic acid, 2-(4-chloro-2-methylphenoxy)propionic acid, 2-methyl-4-chlorophenoxyacetic acid, penicillin G sodium salt, amoxicillin sodium, and ampicillin sodium were purchased from Shanghai Macklin Biochemical Co., Ltd. (Shanghai, China).

Instruments

An ultrasonic microwave synergistic reaction workstation (Nanjing Xianou XO-SM100, China) was used throughout the whole study. Fourier transform infrared (FT-IR) spectroscopy was monitored on a Nicolet IR AVATAR-360 spectrometer (Nicolet, USA) with pure KBr as background. Scanning electron microscopy (SEM) was performed on a Gemini SEM-500 (ZEISS, Germany). Transmission electron microscope (TEM) images were collected from a JEOL-100CXII microscope (JEOL, Japan). The solid ^{13}C nuclear magnetic resonance (^{13}C-NMR) spectra were recorded on the Infinityplus 300 (VARIAN, USA). The thermogravimetric analysis (TGA) was

analyzed on a PTC-10A thermal gravimetric analyzer (Rigaku, Japan) under air from room temperature to 700 °C. The N_2 adsorption-desorption isotherms were obtained on an ASAP 2010 micropore physisorption analyzer (Micromeritics, Nor-cross, GA, USA). The water contact angle measurements were carried out on a PZ-200SD optical contact angle measuring device (PINZHICS, China). The total organic carbon (TOC) was determined on TOC-L CPH (SHIMADZU, Japan). The ion chromatography analysis was performed on Feld ICS5000+ (Thermo, USA). The size distribution was measured on a Nano ZS zetasizer (Malvern Panalytical, UK).

The HPLC anatysis was performed on an LC3000N HPLC system (CXTH, China). A CO-5060 column heater (Ameritech, USA) was used to control the column temperature. A WondaSil C18 (250 mm × 4.6 mm, 5 μm) column was applied to determine the concentration of the studied analytes. The mobile phase was methanol: acetonitrile: 0.02 mol L^{-1} oxalic acid = 1:2:7 at a flow rate of 1 mL min^{-1}. UV detector wavelength was set as 365 nm.

Adsorption kinetics

The adsorption capacity of TCH on US-MONs can be calculated by Eq. (1):

$$q_t = \frac{(C_0 - C_t)v}{m} \tag{1}$$

where C_0 and C_t (mg L^{-1}) are the concentrations of TCH at initial and time t (min), respectively, and q_t (mg g^{-1}) is the absorption capacity of TCH at time t. The v (mL) is the solution volume of TCH and the m (mg) is the dosage of US-MONs.

The pseudo-first-order kinetic equation is given as Eq. (2):

$$\ln(q_e - q_t) = lnq_t - K_1 t \tag{2}$$

where q_e is the adsorption capacity (mg g^{-1}) at equilibrium. K_1 (h^{-1}) is the pseudo-first-order rate constant. q_t (mg g^{-1}) is the amount of adsorption at time t (h).

The pseudo-second-order kinetic equation is given as Eq. (3):

$$\frac{t}{q_t} = \frac{1}{K_2 q_e^2} + \frac{t}{q_e} \tag{3}$$

where q_e (mg g^{-1}) is the adsorption capacity at equilibrium. K_2 (g mg^{-1} min^{-1}) is the pseudo-second-order rate constant. q_t (mg g^{-1}) is the amount of adsorption at time t (min).

The Elovich model is similar to the pseudo-second-order model, which is expressed as Eq. (4):

$$q_t = \frac{1}{\beta} lnt + \frac{1}{\beta} ln(\alpha\beta) \tag{4}$$

where q_t (mg g^{-1}) is the amount of adsorption at time t (h). α (mg g^{-1} h^{-1}) is the initial adsorption rate constant, and β (g mg^{-1}) is a parameter related to the surface coverage of the adsorbent and the activation energy of chemical adsorption.

For the intra particle diffusion model, the adsorption process can be expressed as Eq. (5):

$$q_t = K_i t^{0.5} + C \tag{5}$$

where K_i (mg g^{-1} $h^{-0.5}$) is the particle internal diffusion constant and C (mg g^{-1}) is a constant proportional to the thickness of the boundary layer.

Adsorption isotherms

The Langmuir adsorption model was used to evaluate the adsorption behavior, which can be expressed as Eq. (6):

$$\frac{C_e}{q_e} = \frac{1}{bq_0} + \frac{C_e}{q_0} \tag{6}$$

where C_e (mg L^{-1}) is the concentration of TCH at equilibrium, q_e and q_0 (mg g^{-1}) are the equilibrium and maximum adsorption capacities, respectively, and b (L mg^{-1}) is the Langmuir constant.

The separation factor (R_L), a dimensionless constant, can be defined as Eq. (7):

$$R_L = \frac{1}{1 + bC_0} \tag{7}$$

where b (L mg^{-1}) is the Langmuir constant, C_0 (mg L^{-1}) is the initial concentration of TCH.

It is possible to calculate the thermodynamic free energy change (ΔG, kJ mol^{-1}), enthalpy change (ΔH, kJ mol^{-1}), and entropy change (ΔS, J mol^{-1} K^{-1}) related to the adsorption process according to Eq. (8 and 9):

$$lnK_0 = \frac{\Delta S}{R} - \frac{\Delta H}{RT} \quad (8)$$

$$\Delta G = -RTlnK_0 \quad (9)$$

where R (J mol^{-1} K^{-1}) is the universal gas constant, T (K) is the absolute temperature, and K_0 is the Langmuir constant.

The Freundlich model was adopted to investigate the adsorption behavior, which can be expressed as Eq. (10):

$$lnq_e = \frac{1}{n}lnC_e + lnK_F \quad (10)$$

where C_e (mg L^{-1}) is the concentration of TCH at equilibrium, q_e (mg g^{-1}) is the equilibrium adsorption capacity, and K_F (L mg^{-1}) and n are Freundlich constants, which indicate the relative adsorption capacity and strength, respectively.

The Tempkin model was applied to evaluating the adsorption behavior, which can be expressed as Eq. (11):

$$q_e = \frac{RT}{b_T}lnA_T + \frac{RT}{b_T}lnC_e \quad (11)$$

where C_e and q_e are the TCH concentration and adsorption capacity at equilibrium, A_T (L g^{-1}) is the equilibrium binding constant and b_T (J mol^{-1}) is the heat of adsorption related constant.

The Dubinin-Radushkevich model was applied to evaluate the adsorption process, which can be expressed as Eq. (12-14):

$$lnq_e = lnq_s - k_{ad}\varepsilon^2 \quad (12)$$

$$\varepsilon = RTln(1 + \frac{1}{C_e}) \quad (13)$$

$$E = \frac{1}{\sqrt{2k_{ad}}} \quad (14)$$

where q_s (mg g^{-1}) is the maximum adsorption capacity, k_{ad} (mol^2 J^{-2}) is the adsorption energy constant and E (kJ mol^{-1}) is the average free energy.

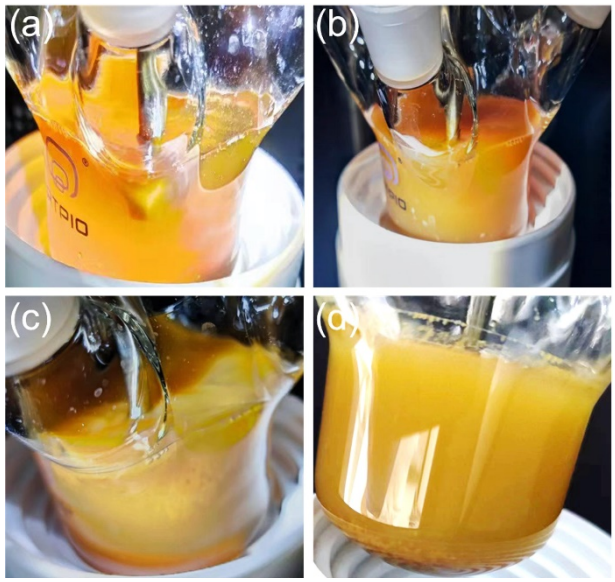

Fig. S1. Images of US-MON synthesized under different ultrasonic time at 500 W: (a) 0 min (b) 5 min (c) 10 min, and (d) 30 min.

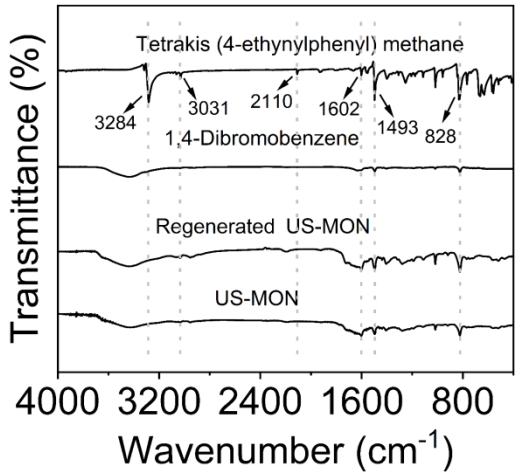

Fig. S2. FT-IR spectra of the monomers, fresh and regenerated US-MON.

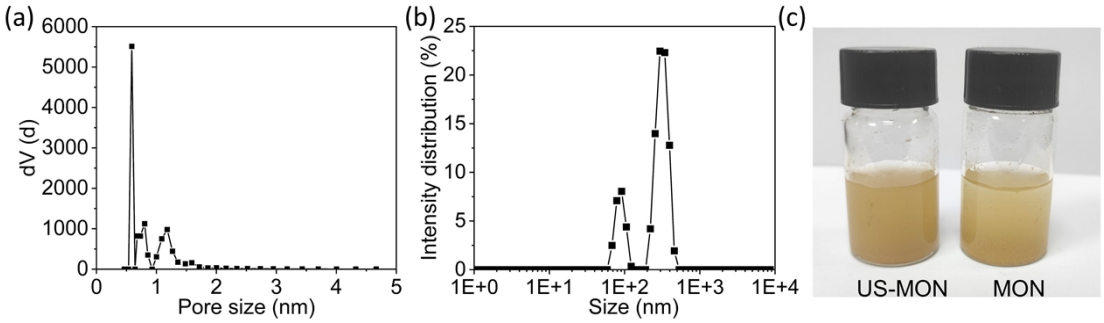

Fig. S3. (a) Pore size distribution of US-MON; (b) size distribution of US-MON; (c) digital images of US-MON and MON after stirring in water.

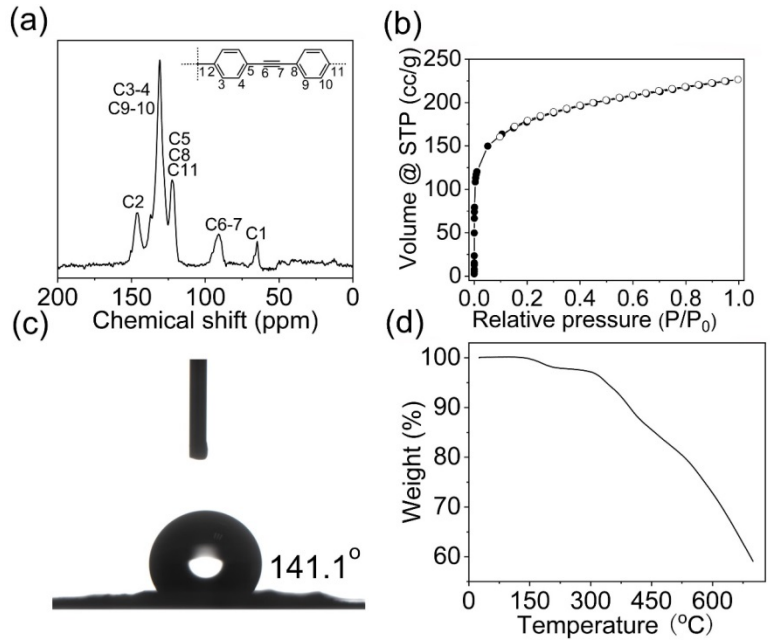

Fig. S4. (a) Solid ^{13}C NMR spectrum, (b) N_2 adsorption-desorption isotherms, (c) water contact angle, and (d) TGA curve of MON synthesized via solvothermal method.

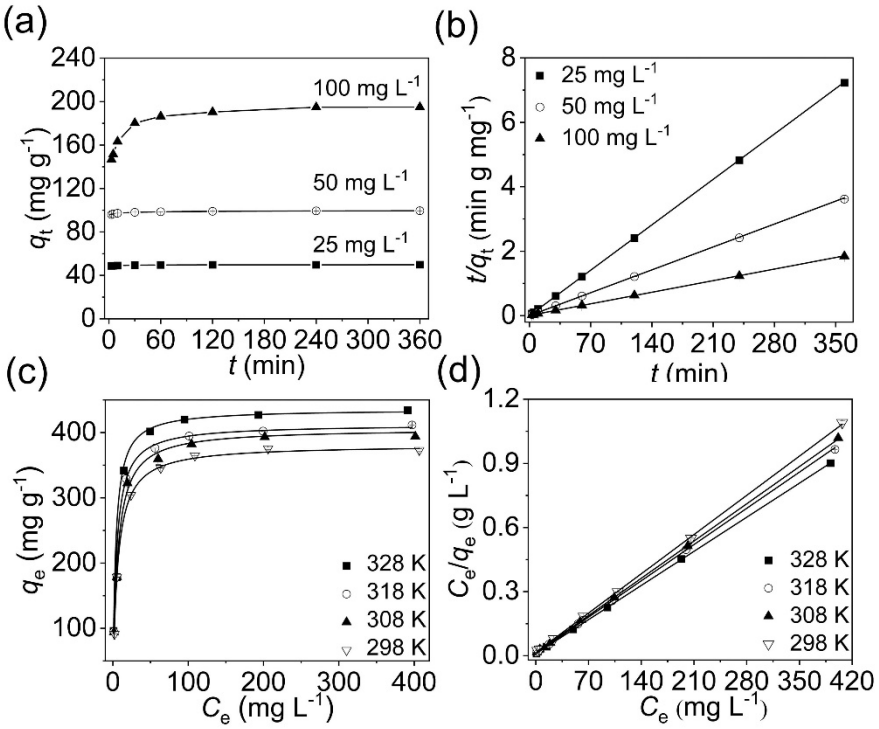

Fig. S5. (a) The adsorption capacity of TCH on MON at different contacting time; (b) pseudo-secondary kinetic curves of TCH on MON; (c) adsorption isotherms of TCH on MON and (d) their corresponding Langmuir plots.

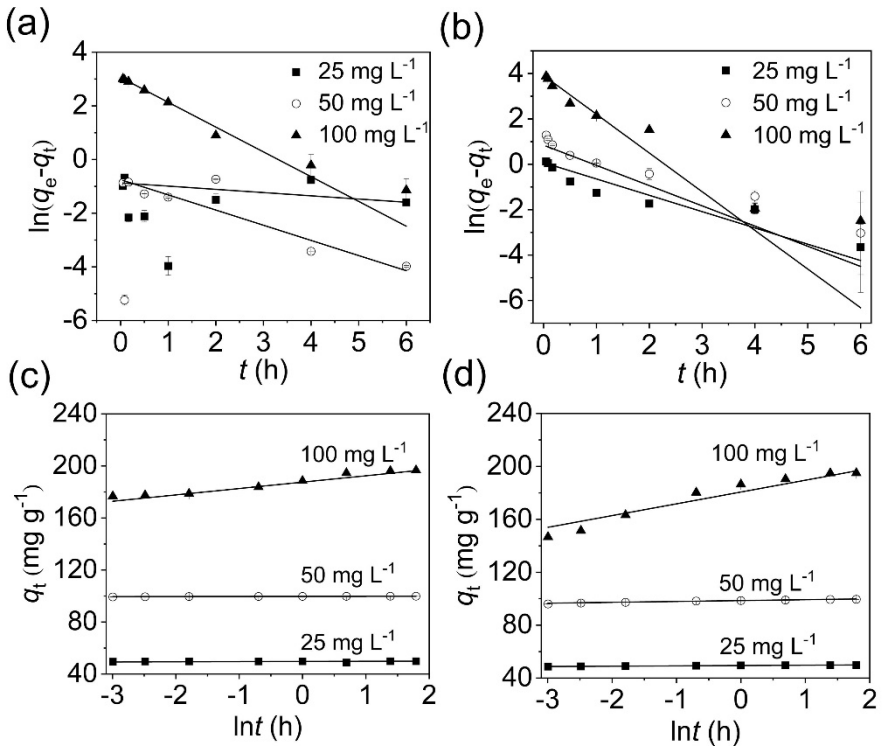

Fig. S6. Pseudo-first-order kinetics plots for the adsorption of TCH on (a) US-MON, and (b) MON. Elovich plots for the adsorption of TCH on (c) US-MON, and (d) MON.

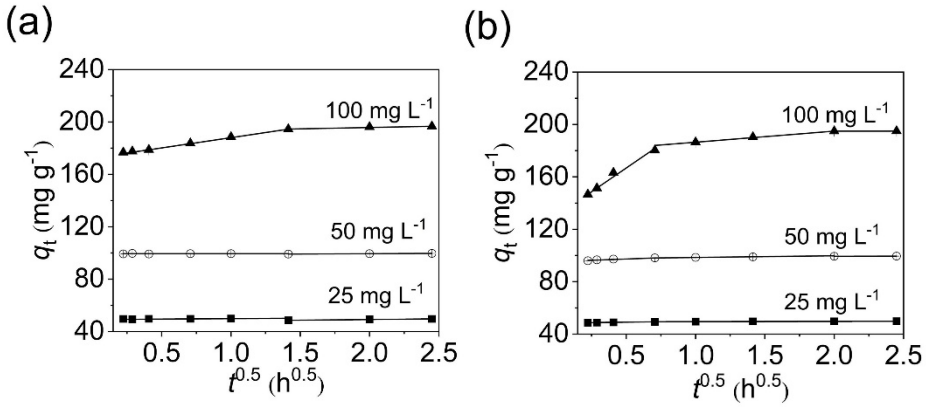

Fig. S7. Intraparticle diffusion model for the adsorption of TCH on (a) US-MON, and (b) MON.

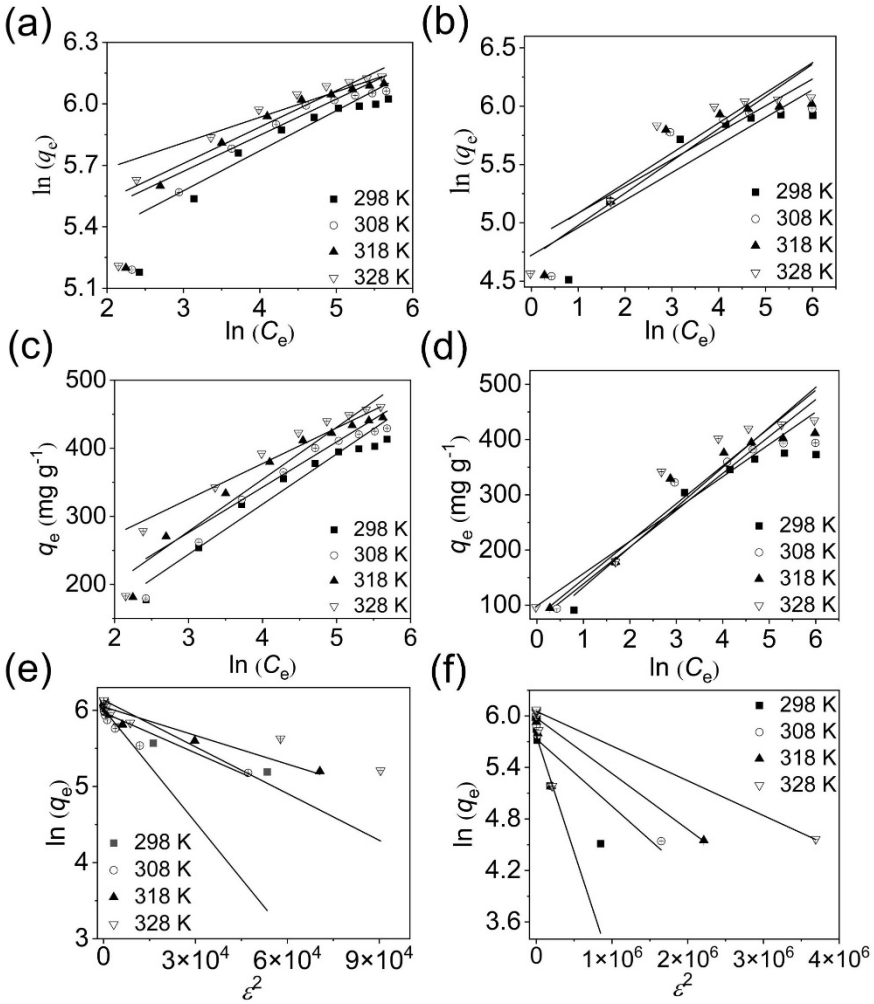

Fig. S8. (a) Freundlich, (c) Tempkin and (e) Dubinin-Radushkevich plots for the adsorption of TCH on US-MON. (b) Freundlich, (d) Tempkin, and (f) Dubinin-Radushkevich plots for the adsorption of TCH on MON.

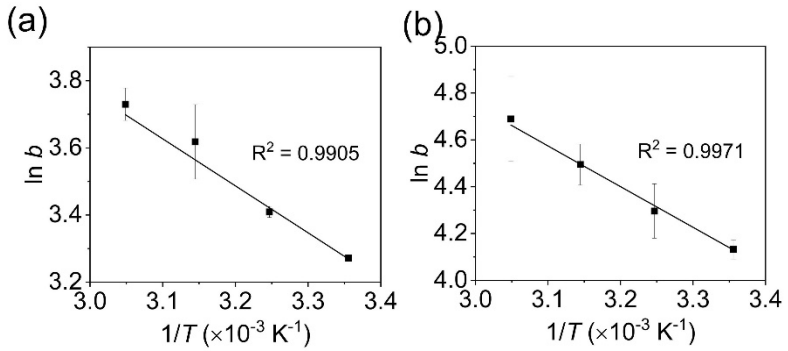

Fig. S9. Van't Hoff plots for the adsorption of TCH on (a) US-MON, and (b) MON.

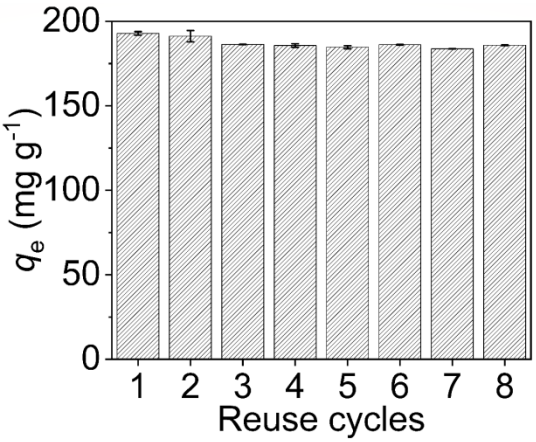

Fig. S10. Reuse cycles of US-MON for the desorption of TCH (100 mg L^{-1}).

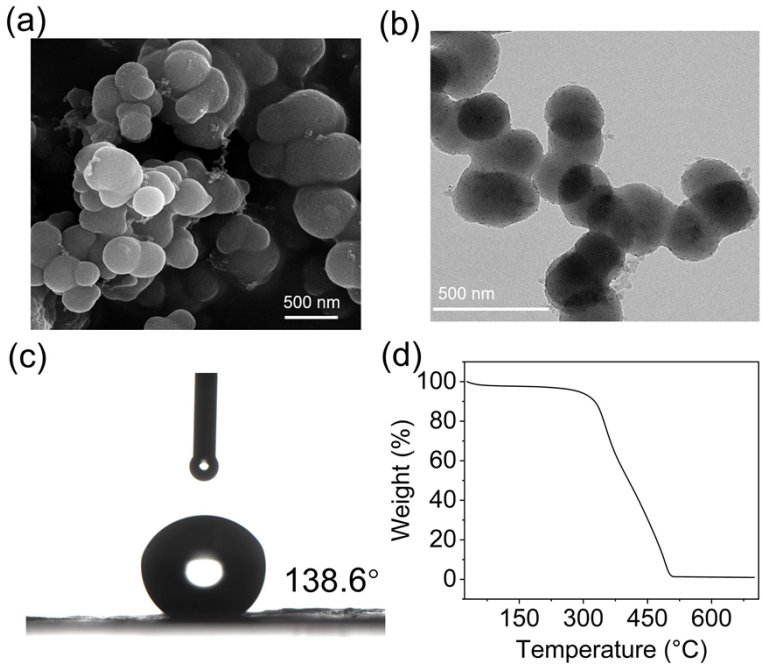

Fig. S11. (a) SEM, (b) TEM, (c) water contact angle, and (d) TGA curve of regenerated US-MON after 8 adsorption-desorption cycles.

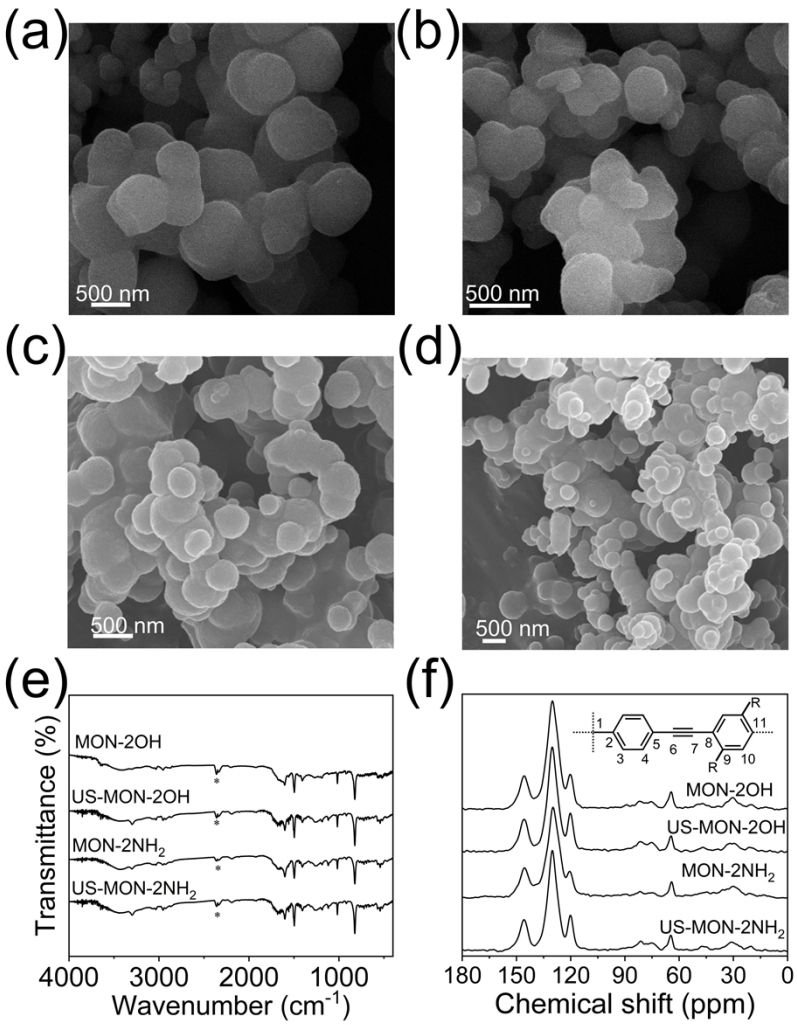

Fig. S12. SEM of (a) MON-2NH_2, (b) US-MON-2NH_2, (c) MON-2OH, (d) US-MON-2OH. (e) FT-IR and (f) ^{13}C NMR spectra of MONs.

Table S1. Pseudo-first-order kinetic parameters of TCH on US-MON and solvothermal synthesized MON.

	C_0 (mg L^{-1})	$q_{e,exp}$ (mg g^{-1})	Pseudo-first-order kinetic parameters		
			K_1 (h^{-1})	$q_{e,cal}$ (mg g^{-1})	R^2
US-MON	25	49.88	0.120	0.4	0.967
	50	99.71	0.565	0.5	0.826
	100	197.00	0.924	21.3	0.904
MON	25	49.88	0.719	1.1	0.762
	50	99.61	0.891	2.3	0.790
	100	195.00	1.706	50.2	0.986

Table S2. Elovich parameters of TCH on US-MON and solvothermal synthesized MON.

	C_0 (mg L^{-1})	α (mg g^{-1} h^{-1})	β(g mg^{-1})	R^2
US-MON	25	-	8.2	0.235
	50	-	16.1	0.888
	100	2.14×10^{17}	0.2	0.936
MON	25	-	4.0	0.972
	50	3.42×10^{64}	1.5	0.974
	100	5.76×10^{9}	0.11	0.901

Table S3. Intraparticle diffusion parameters of TCH on US-MON and solvothermal synthesized MON.

	C_0 (mg L^{-1})	K_{i1} (mg g^{-1} $h^{-0.5}$)	c_1	R^2	K_{i2} (mg g^{-1} $h^{-0.5}$)	c_2	R^2
US-MON	25	0.66 ± 0.10	49.20	0.909	1.04 ± 0.10	47.14	0.990
	50	0.18 ± 0.02	99.45	0.993	0.49 ± 0.02	98.44	0.998
	100	15.65 ± 0.76	172.36	0.991	2.05 ± 0.26	191.68	0.984
MON	25	1.39 ± 0.02	48.43	0.999	0.24 ± 0.07	49.29	0.990
	50	3.91 ± 0.43	95.36	0.977	1.29 ± 0.17	97.22	0.998
	100	72.41 ± 4.60	130.52	0.992	8.46 ± 0.23	177.98	0.998

Table S4. The R_L values calculated from the Langmuir isotherms of US-MON for TCH.

C_0 (mg L^{-1})	100	150	200	250	300	350	400	450	500
328 K	0.104	0.072	0.055	0.045	0.037	0.032	0.028	0.025	0.023
318 K	0.114	0.079	0.061	0.049	0.041	0.036	0.031	0.028	0.025
308 K	0.130	0.091	0.070	0.057	0.048	0.041	0.036	0.032	0.029
298 K	0.142	0.100	0.077	0.062	0.052	0.045	0.040	0.036	0.032

Table S5. Freundlich parameters of TCH on US-MON and solvothermal synthesized MON.

	Freundlich parameters			
	T (K)	K_F (L mg^{-1})	n	R^2
US-MON	298	146.86	5.12	0.812
	308	171.04	5.67	0.989
	318	177.21	5.64	0.724
	328	229.74	8.04	0.942
MON	298	124.61	3.88	0.887
	308	128.16	4.35	0.745
	318	110.22	3.62	0.896
	328	112.37	4.23	0.910

Table S6. The Tempkin and Dubinin-Radushkevich parameters for the adsorption of TCH on US-MON and solvothermal synthesized MON.

		Tempkin parameters			Dubinin-Radushkevich parameters			
	T (K)	A_T (L g^{-1})	b_T (J mol^{-1})	R^2	q_s (mg g^{-1})	k_{ad} (mol^2 J^{-2})	E (kJ mol^{-1})	R^2
US-MON	298	1.37	33.63	0.948	409.57	4.95×10^{-5}	0.100	0.879
	308	3.94	39.51	0.993	391.86	1.77×10^{-5}	0.168	0.850
	318	1.90	34.63	0.913	422.50	1.25×10^{-5}	0.199	0.936
	328	25.31	52.23	0.967	461.38	2.05×10^{-5}	0.156	0.710
MON	298	2.30	34.23	0.967	319.41	2.70×10^{-6}	0.430	0.879
	308	2.93	38.35	0.927	308.91	7.85×10^{-7}	0.798	0.850
	318	3.15	38.62	0.995	394.83	6.49×10^{-7}	0.878	0.936
	328	5.42	46.62	0.988	426.28	4.05×10^{-7}	1.111	0.710

Table S7. Concentration (mg L^{-1}) of total organic carbon (TOC) and Cl^-, HCO_3^-, and SO_4^{2-} in lake water sample before and after adsorption with US-MON.

Lake water sample	Cl^-	SO_4^{2-}	HCO_3^-	TOC
Before adsorption	44.62	62.26	49.27	34.70
After adsorption	44.17	62.67	47.66	25.32

Table S8. Comparison of BET surface area, pore volume, maximum adsorption capacity based on Langmuir model for TCH, and water contact angle of MONs.

	BET (m^2 g^{-1})	Pore volume (cc g^{-1})	q_0 (mg g^{-1})	water contact angle (°)
MON	647.6	0.432	401.6	141.1
US-MON	1030.9	0.389	437.4	138.3
MON-2OH	1040.0	0.575	515.5	142.6
US-MON-2OH	1090.7	0.489	520.8	143.5
MON-2NH_2	946.7	0.888	502.5	144.2
US-MON-2NH_2	1078.6	0.811	507.6	145.9

Table S9. The adsorption capacity of different analytes (100 mg L^{-1}) on US-MON at 25 °C.

Analytes	q_e (mg g^{-1})
cefotaxime sodium	84.1
cefixime	39.2
cefuroxime sodium	73.7
cefazolin sodium salt	111.2
dichlorprop	134.2
2,4-dichlorophenoxyacetic acid	135.5
2-(4-chloro-2-methylphenoxy)propionic acid	119.9
2-methyl-4-chlorophenoxyacetic acid	101.1
penicillin G sodium salt	80.0
amoxicillin sodium	32.4
ampicillin sodium	59.6
enrofloxacin	182.2
ofloxacin	191.1
ciprofloxacin	186.0
enoxacin	180.2
TCH	197.0